iScience

CellPress
OPEN ACCESS

Article

Hovering flight regulation of pigeon robots in laboratory and field

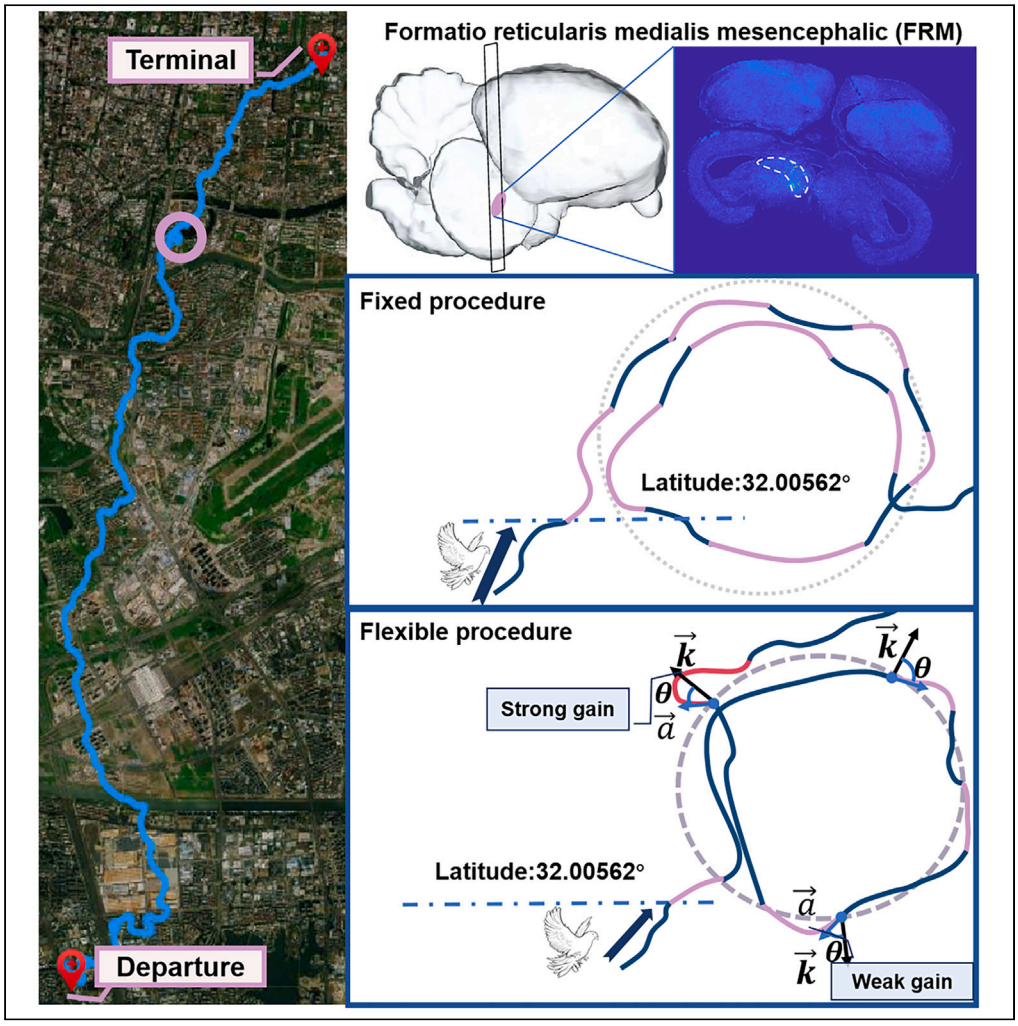

Zhengyue Zhou, Yezhong Tang, Rongxun Li, Wenbo Wang, Zhendong Dai

wwb523@nuaa.edu.cn (W.W.)
zddai@nuaa.edu.cn (Z.D.)

Highlights

Upgraded energy efficiency of SGD gathering comprehensive data

The modulation effectiveness of PW gain was tested in both laboratory and field

Achievement of fixed and flexible navigation procedures

Stable circle curvature and high success rate when hovering over specific landmarks

Zhou et al., iScience 27, 110927
October 18, 2024 © 2024
Published by Elsevier Inc.
https://doi.org/10.1016/j.isci.2024.110927

iScience

CellPress
OPEN ACCESS

Article

Hovering flight regulation of pigeon robots in laboratory and field

Zhengyue Zhou,[1] Yezhong Tang,[1,2] Rongxun Li,[1] Wenbo Wang,[1,3,*] and Zhendong Dai[1,*]

SUMMARY

Compared to traditional bio-mimic robots, animal robots show superior locomotion, energy efficiency, and adaptability to complex environments but most remained in laboratory stage, needing further development for practical applications like exploration and inspection. Our pigeon robots validated in both laboratory and field, tested with an electrical stimulus unit (2-s duration, 0.5 ms pulse width, 80 Hz frequency). In a fixed stimulus procedure, hovering flight was conducted with 8 stimulus units applied every 2 s after flew over the trigger boundary. In a flexible procedure, stimulus was applied whenever they deviated from a virtual circle, with pulse width gains of 0.1 ms or 0.2 ms according to the trajectory angle. These optimized protocols achieved a success hovering rate of 87.5% and circle curvatures of 0.008 m–1–0.024 m-1, largely advancing the practical application of animal robots.

INTRODUCTION

Animal robots are referred to animal-machine hybrid systems with organisms as vectors and advanced as the technological development of the bio-machine interface to galvanize motion behaviors. Animal intelligence and behavior have evolved over hundreds of millions of years; their superiority can be used in animal robots to move freely in complex environments.[1] Therefore, the animal robot has advantages over traditional robots, such as the massive size of bulk,[2] heat generation,[3] algorithm density,[4] and self-energizing and temporary battery duty.[5] As a result of its outstanding advantages, the hybrid system has been developed widely in several species of insects,[6] teleost,[7] reptiles,[8] mammals,[9,10] and birds.[1]

Although controls of animal robot navigation in the laboratories have succeeded in several species, such as the flight regulation of beetle robots,[11] multi-scenes behavior adjustment of rat robots based on a visual fusion system,[12] and open field guidance of pigeon robots,[1] the behavior regulation out of the laboratory is restricted significantly by technical challenges.[13] The existed stimulus generation device (SGD) lacked of ability to collect animal posture and location information[14]; at the stage out of the laboratory, information on integrated posture and location is impending demands for precise animal robot navigation.[9,15] In outdoor navigation, human-designed signals often guide locomotion behaviors against the voluntary movement of animals, resulting in less robustness in the motion control of animal robots. Thus, it will be a priority in designing stimulus protocol to reduce the conflict between the animal willingness and command orders emitted by experimenters to navigate the animal robots in highly urbanized external environments with complex topography.

This study focused on the adjustments of locomotion behaviors with the pigeons as vectors. In contrast with other animals,[16] pigeons have excellent spatial navigation abilities, thus being able to conduct survey tasks on long distances and large scales with artificial guidance. Initially, we innovated SGD to enhance performance with high stimulation precision and lessen the energy consumption for elongating navigation. As a medium for harmonizing the external demands with the animal's internal cognition, the upgraded SGD could record the posture and location information of the carriers in real-time. Moreover, this device could regulate locomotive behaviors on various experimental subjects, such as rats or mice, during indoor and outdoor tasks. To promote the practical application of pigeon robots under urban circumstances, we designed two behavioral adjustment procedures for hovering motion control.

RESULT

Nuclei for turning behavior regulation

Based on previous researches[1,17–20], the current work tried to control the outdoor flights of pigeon robots by applying electric stimulation in both nuclei Formatio Reticularis Medialis mesencephalic (FRM)[21–25] and Locus Coeruleus (LoC)[26–31] (see Figure S1A). FRM in the pigeon is the homology of mesencephalic locomotion region (MLR)[21,22] in the rats, which is a motor neuron pool at the mixture area which receives projections from the basal ganglia and cortex and projects to the spinal cord.[30,31] The FRM was demonstrated to be involved in the navigation behaviors of the pigeon, such as straightforward locomotion and turning left and right. The LoC has multi-connections to the telencephalon,

[1]Institute of Bio-inspired Structure and Surface Engineering, Nanjing University of Aeronautics and Astronautics, Nanjing, Jiangsu, China
[2]Chengdu Institute of Biology, Chinese Academy of Sciences. No.9 Section 4, Renmin Nan Road, Chengdu 610041, Sichuan, China
[3]Lead contact
*Correspondence: wwb523@nuaa.edu.cn (W.W.), zddai@nuaa.edu.cn (Z.D.)
https://doi.org/10.1016/j.isci.2024.110927

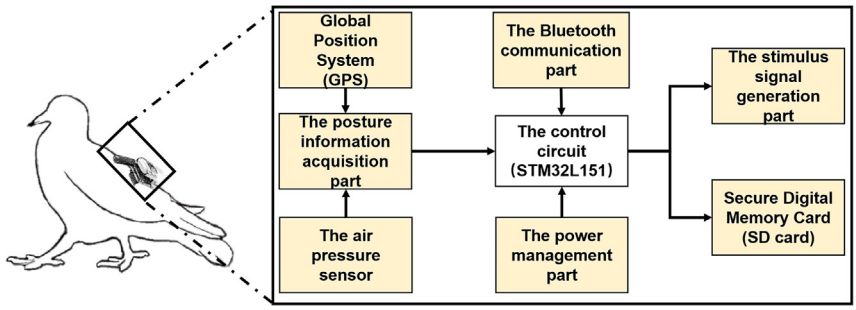

Figure 1. The schematic graph of the stimulus generation device

thalamus, mesencephalon, and spinal cord, and then can modulate the locomotion speeding up and slowing down.[24–27,32,33] It was proposed to initiate the motions like take-off in pigeons.

During the surgery, we implanted four or more electrodes with 130 μm diameters into specific nuclei, FRM (Ap: 3.45 mm; ML: ±1.40 mm) and LoC (Ap: 1.95 mm; ML: ±1.50 mm). The implantation operation of electrodes for stimulation or injection was completed by placing the pigeon heads on the brain stereotaxis. With an injection of the golden neuro-fluorescence, brain sections with the sites of golden staining were used to position the pigeon's FRM and LoC by matching to the standard atlas of the pigeon brain.

Design and test of stimulus generation device

The SGD includes five major components (Figure 1): information acquisition of posture and location, stimulus signal generation, Bluetooth communication/pre-programmed instruction sets, and power management. (1) The posture and location information was acquiesced by integrating the Global Position System (GPS) module for the collection of latitude and longitude coordinates and an air pressure sensor for altitude. All information is stored on the secure digital memory card. (2) The stimulation generation module could output a range of 0∼3.3 voltages with a resolution of 0.804mV (STAR Methods) with a 12-bit D\A conversion port as the signal source. (3) The wireless communication between the host computer and the slave computer was conducted by ATK-BLE01 Bluetooth serial port module which was integrated into SGD to modify the stimulus signal parameters and validate the pigeon robot's responses. Of the energy module, the maximum transmitting power was + 8 DBM, and the transmission distance in the open field reached up to 100 m, satisfying the indoor tests. (4) The stimulation instruction sets were generated in the field in pre-programmed mode. (5) An amplifier circuit was designed to convert the 0∼3.3V voltages into −3.3V–3.3V voltages, and electrostatic discharge (ESD) protection was added to the power socket to filter out static electricity. The overall size of our SGD was 2.7 × 2.3 × 1.3 cm^3, with a total mass of 13.0 g.

To verify the effectiveness and practicability of SGD (see Figures S3A and S3C), we tested indoor the functions of stimulation signal generation, Bluetooth communication, and power management. The navigation instructions for the pigeon robots were generated on the Bluetooth protocol. For instruction set "IBSS, 01, 3.0, 0.5," here IBSS acted as a check code and when it was detected, the signal was recognized as a valid instruction. Then, 01 represented the current communication channel sequence number; 3.0 the amplitude of the stimulus signal in voltage; 0.5 (ms) the pulse width of the signal. To verify whether the device communicates effectively with the host computer and outputs accurate signals, the mobile phone (Android System) was used as the host computer to send the manual instruction to SGD which, in turn, outputted stimulating signals to pigeon robots. The results indicated that SGD could output preset commands in a given order, presenting "IBSS, 01, 3.0, 0.5" (see Figure S3D). In addition, the acquisition functions of posture and location information were tested in the Ming Palace Campus of the Nanjing University of Aeronautics and Astronautics, where SGD was carried manually to move repetitively from building A12 (Departure) to the East Gate (Terminal). After multiple recordings on the fixed pathway, it resulted that the average GPS positioning error in the horizontal plane was less than 15 m, and the average error of height resolution was less than 0.2 m (see Figure S3B).

Determination of stimulation amplitude

It is well known that the stimulus amplitude, pulse width, pulse number, frequency, and other parameters have different effects on the behavior regulation of the pigeon robot, such as that the locomotion activity could be promoted by elevating the stimulus amplitude.[13,34] Four electrodes were implanted simultaneously at the midbrain nuclei of the pigeon robot (STAR Methods). To verify whether electrodes were implanted correctly, awake pigeons were released in the open field and guided by the instruction set. Only if a pigeon could display corresponding behaviors under the guidance of the instruction set in all implanted sites, this subject would be deemed suitable for further experiments. Six pigeons, named W036, R012, Y074, W064, R069, and B074, were finally selected as the robot vectors used in the subsequent analyses (STAR Methods). The result showed that the threshold of electoral stimulation to induce a response was set at 1.0 V for all implanted sites in six pigeon robots. The responsive level tended to increase with the increasing amplitude of stimulus electricity at the free and awake state, showing that the moving behaviors of six pigeon robots could be stably and effectively controlled. Therefore we have established the optimized amplitudes of voltages with which fidelity responses could be induced under the awake free-moving state for all individuals of the pigeon robots (Table 1).

Table 1. The optimum parameters of individual pigeon robots

Pigeon Robots	Stimulation mode	Amplitude (V) (Left)	Amplitude (V) (Right)	Frequency (Hz)	Pulse (ms)	Duty cycle (%)
W036	Instruction set	1.2	2.4	80	0.5	50
R012	Instruction set	2.6	2.3	80	0.5	50
Y074	Instruction set	1.8	2.1	80	0.5	50
W064	Instruction set	1.5	1.9	80	0.5	50
R069	Instruction set	2.5	2.9	80	0.5	50
B074	Instruction set	3.0	1.8	80	0.5	50

Optimization of stimulation pulse width (PW)

The stimulus PW is of superiority over electric amplitude in adjusting locomotion smoothly. With optimized PWs, the pigeons could be forced to move around the target by continuously stimulating signals, released from the given site.[17] The same six pigeon robots were involved in this experimental phase. At the laboratory, pigeon robots were driven to turn successfully counterclockwise and clockwise circles by stimulations with fixed amplitude and varied PW (0.5 ms, 0.7 ms, and 0.9 ms) and stimulus number (STAR Methods) (Figure 2A). As Figures 2C and 2D shows, both PWs and stimulus numbers have contributed significantly to the turning success rate. Effects of 0.2 ms PW gain, with PWs increasing from 0.5 ms to 0.9 ms, could be compensated with the inclement of stimulus numbers and then, resulted in numbers increase of successful circle turnings (Figures 2B and S4B–S4D). Even so, there is no significant difference in stimulus numbers required to accomplish a circle turning for each PW among pigeon individuals (Table 2). The regularity of stimulations was very important for outdoor tests because the individual variations could lead to uncertainty in the behavior adjustment with similar stimulus parameters, showing that the motion behaviors of the pigeon robots can be precisely adjusted by PW.

Formation of flight pathways

Since the outdoor locomotion of pigeon robots was controlled by pre-programmed mode, the flight pathway would serve as a standard route along which the fixed-points for hovering could be selected offline previously (Figure 3A). Fortunately, the pigeon individuals generally flew in relatively fixed trajectories during their homing. A total 6 pigeons were equipped with our device and released at (Longitude 118.78303, Latitude 31.94400°), 9.2 km from the home cage. Each animal was trained to fly 20 times, 11 flights without and 9 with the device, recording its routes by acquisition subsystem of posture and location information.

The pathway deviations of the last 6 trials out of 9 training flights with the device were analyzed along the routes by the standard deviation analysis (STAR Methods). By calculating the Euclidean distance of each pair of two adjacent points on the flight trajectory, the total length of flight pathways and each trial of each pigeon robot were computed, respectively, and the routes of each individual were projected onto the local map (Figure 3B). Although there were deviations in the flight pathways between pigeon robots, their respective flights remained generally in fixed pathways with SD < 1 (Figure 3B; Table 3). The longitude deviations from its average pathway were measured to be less than 55.5 m at the trigger site for all subjects. To build a trigger boundary across the pathways at the given site, lines of 111 m along the longitude coordinates were drawn based on the six trials (Figure 3B).

Two experimental procedures were designed and implemented in this phase with six pigeon robots which were promoted to perform smooth hovering within a relative restrict circle location. Procedure 1 (Figure 4A) involved the fixed stimulus paradigm and included three pigeon robots, W036, R012, and Y074. Procedure 2 with the flexible stimulus paradigm (Figure 4B) was designed based on the results from procedure 1, in pigeon robots W064, R069, and B074. The related data were collected with the acquisition subsystem of SGD.

A total of 52 trials were accomplished in three pigeon robots under stimulation procedure 1 (Figures 5A and 5B). The pigeon robots showed that both turning circle curvatures and hovering success rate reduced with the stimulation interval (SI) increased when the duration of stimulation remained unchanged. For all trials, the accomplished circle curvatures ranged from 0.008 m^{-1} to 0.025 m^{-1}, and the achieved hovering success rates were up to 87.5% (Table 4). One-way ANOVA analyses resulted in significant differences in curvatures of turning circles among individuals in response to stimulations with varied SIs, from fixed intervals of 2 s, 2.4 s, 3 s in procedure 1 to flexible intervals in procedure 2 (Tables 4 and 5; Figure 5C). For the hovering success rates, the statistical tests showed similar trends as for the circle curvatures (Figure 5D).

For stimulation procedure 2, a total of 26 trials were included in our statistical tests, and the data were collected as in procedure 1. The statistical results showed that both turning circle curvatures ($p = 0.882$) and hovering success rates ($p = 0.921$) under the same stimulation procedure were not significantly different among individuals (Table 5).

Consideration of outdoor circumstances, individual differences in response to stimuli with varied parameters might unignorably influence the robots' application in practice. In cases of procedure 1, significant differences in two behavioral measures among individuals, i.e., the circle curvature and hovering success rate, were found with three stimulus intervals compared with the results of procedure 2 (Figures 5E and 5F). It was noted that the pigeon robots performed the hovering of circle turns with more even curvatures stimulated by procedure 2. Although the hovering success rate by procedure 2 was less than that by procedure 1, individuals showed their success rates more consistently (Figure 5G). Conclusively, our results favored a fixed stimulus duration with flexible stimulus intervals in outdoor practice.

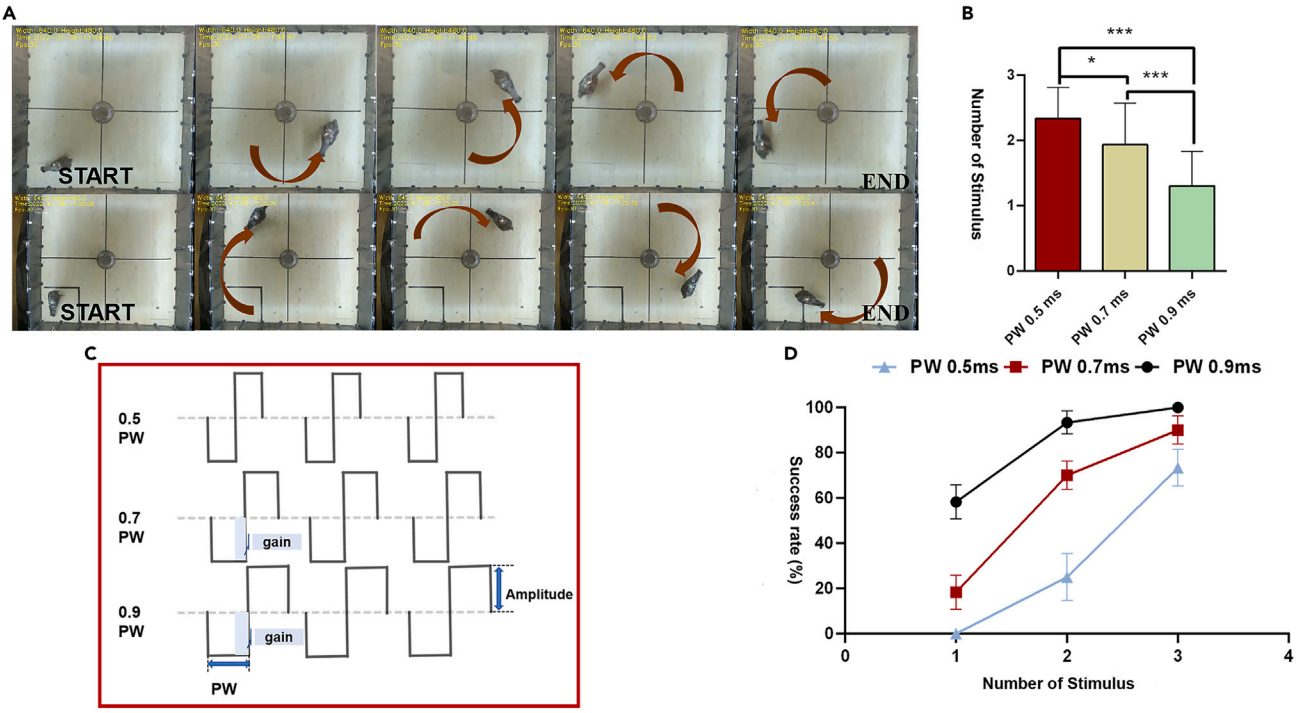

Figure 2. The laboratory test of stimulus PWs and numbers

(A) The real test scene of the open field (counterclockwise and clockwise).

(B) The quantitative comparisons by ANOVA showing relationships between PWs and the number of stimuli in inducing turning behavior.

(C) The schematic diagram for PWs, gain, and amplitude.

(D)The plot of the success rates against the number of stimuli.

DISCUSSION

Animal robots and behavioral regulation

Animal vectors can execute specific tasks in dangerous environments inaccessible to humans by their locomotion abilities gained from biological evolution. With the benefits of the sensory system, flight performance and power utilization, animal robots can accomplish varied tasks more efficiently than traditional robots.[1] Currently, the behavioral regulations of animal robots are generally accomplished by (A) modifying the upper motor neurons in the brainstem or the cord spines related to Central Pattern Generator (CPG)[17]; (B) specifically activating somatosensory perception[35]; (C) using emotional feed backs[19] which improves the effectiveness of guidance.[36] Various categories of animal robots using SGD technology have been developed, including insects, sharks, geckos, pigeons, rats, etc.[7,9,37] Among these, pigeons have particular advantages under the above three paradigms to navigate their flights. Pigeon robots are predominantly characterized by their extensive lifespan, docile temperament, high intelligence, and tenacious vitality, in addition to their extraordinary spatial navigation and long-distance soaring capabilities.[38,39] In the future, with the development of behavioral regulation methods and devices, large-scale scene exploration can be carried out by loading sensors on the pigeon's body, which will significantly contribute to the research of animal robots.[35]

In designing the guidance methods for pigeons in this study, several considerations were taken into account. Currently, techniques for manipulating specific neural nuclei to induce target animal behaviors include electric stimulation for turning behavior, optogenetics for changing posture such as body elongation or grooming, and chemogenetics for shifting normal social behavior Among these methods,

Table 2. The fixation pathway of individual pigeon robots

	Pigeon Robots	W036	R012	Y074	W064	R069	B074	Mean
PW 0.5	Stimulus times	2.2	2.4	2.3	2.1	2.4	2.6	2.333
	$p > 0.05$ s	0.9524	0.9982	0.9997	0.6067	0.9987	0.4558	–
PW 0.7	Stimulus times	1.9	2.2	1.7	1.8	2.1	1.9	1.933
	$p > 0.05$ s	0.9998	0.7636	0.8550	0.9895	0.9668	0.9998	–
PW 0.9	Stimulus times	1.4	1.2	1.4	1.2	1.1	1.5	1.3
	$p > 0.05$ s	0.495	0.358	0.958	0.358	0.8406	0.8406	–

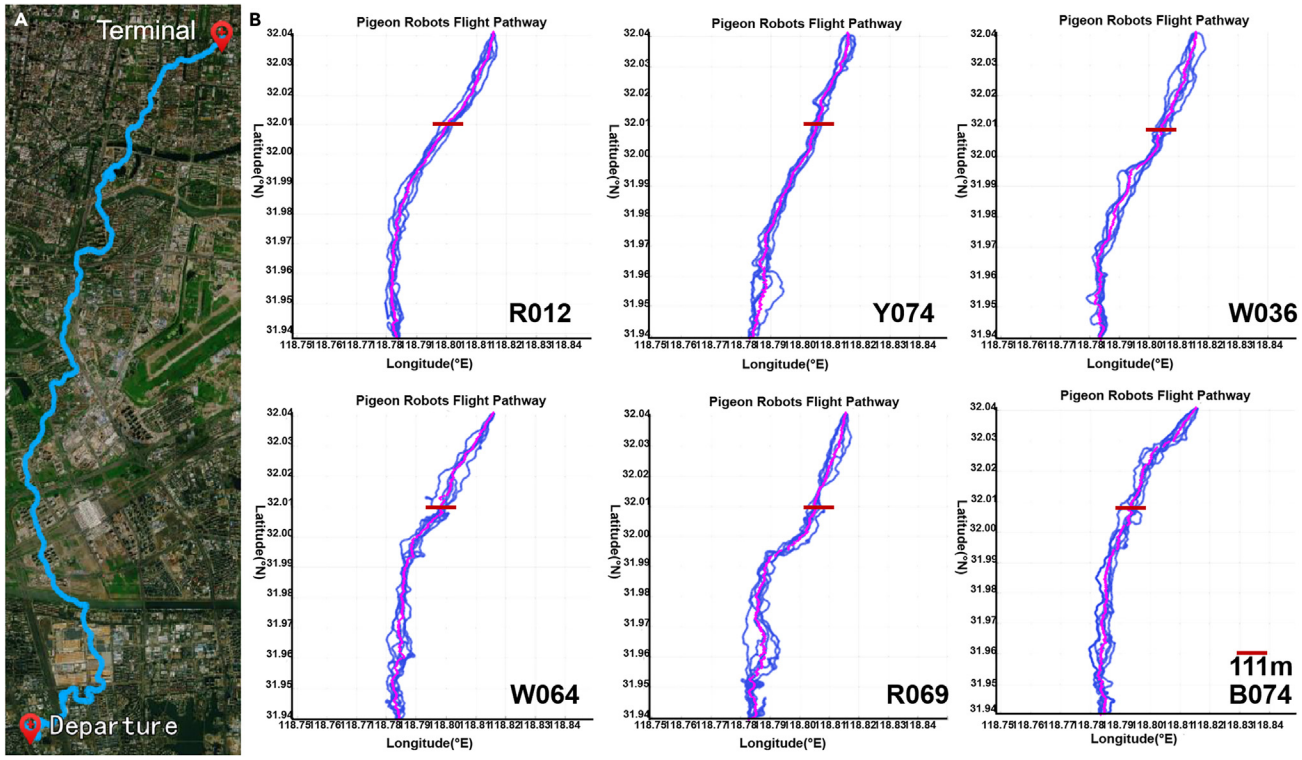

Figure 3. Fixed flight pathways of pigeon robots after training

(A) A typical pathway from the released site to the campus, the violet circle indicating the area for hovering.

(B) The drawing pathways of individuals based on GPS data, the violet lines indicating the average pathways of six flight trials and red bars showing the trigger boundary sites and width.

electric stimulation is a long-standing traditional approach, fast but somewhat imprecise. In designing the guidance methods for pigeons in this study, several considerations were taken into account. Currently, techniques for manipulating specific neural nuclei to induce the mammalian behaviors include electric stimulation for turning behavior, optogenetics for changing posture such as body elongation or grooming,[40] and chemogenetics for shifting normal social behavior.[41,42] Among these methods, electric stimulation is a long-standing traditional approach, fast but somewhat imprecise. These technologies have been successful in the telencephalon in avian studies, yielding many positive results related to visual and auditory functions, as well as social and cognitive processes.[43] Although we failed in express of AAV in the pigeon mesencephalon, this virus can work as the optogenetic tool in the telencephalon of pigeons,[44] telencephalon and diencephalon of zebra finches.[45,46] respectively. It seems in birds that expressions of the viruses and small inert molecules have species- and brain region-specific which did not happen in mammals.

Table 3. Standard deviation coefficient of flight pathway for individual pigeon robot

	Pigeon robots					
Flights (km)	W036	R012	Y074	W064	R069	B074
Trial 1	9.607	9.771	9.485	11.189	9.631	9.517
Trial2	9.648	9.360	9.206	9.718	10.584	9.850
Trial3	9.958	9.576	9.431	9.295	10.301	11.330
Trial4	9.811	9.283	9.120	11.728	10.301	10.236
Trial5	9.407	9.196	11.879	10.115	11.540	11.505
Trial6	10.484	10.442	9.918	10.507	11.048	11.346
Average	9.819	9.605	9.840	10.425	10.568	10.631
SD.	0.343	0.420	0.946	0.832	0.604	0.792
P	0.600	0.600	0.463	0.917	0.916	0.917
coefficient of standard deviation	3.493%	4.376%	9.618%	7.985%	5.724%	7.459%

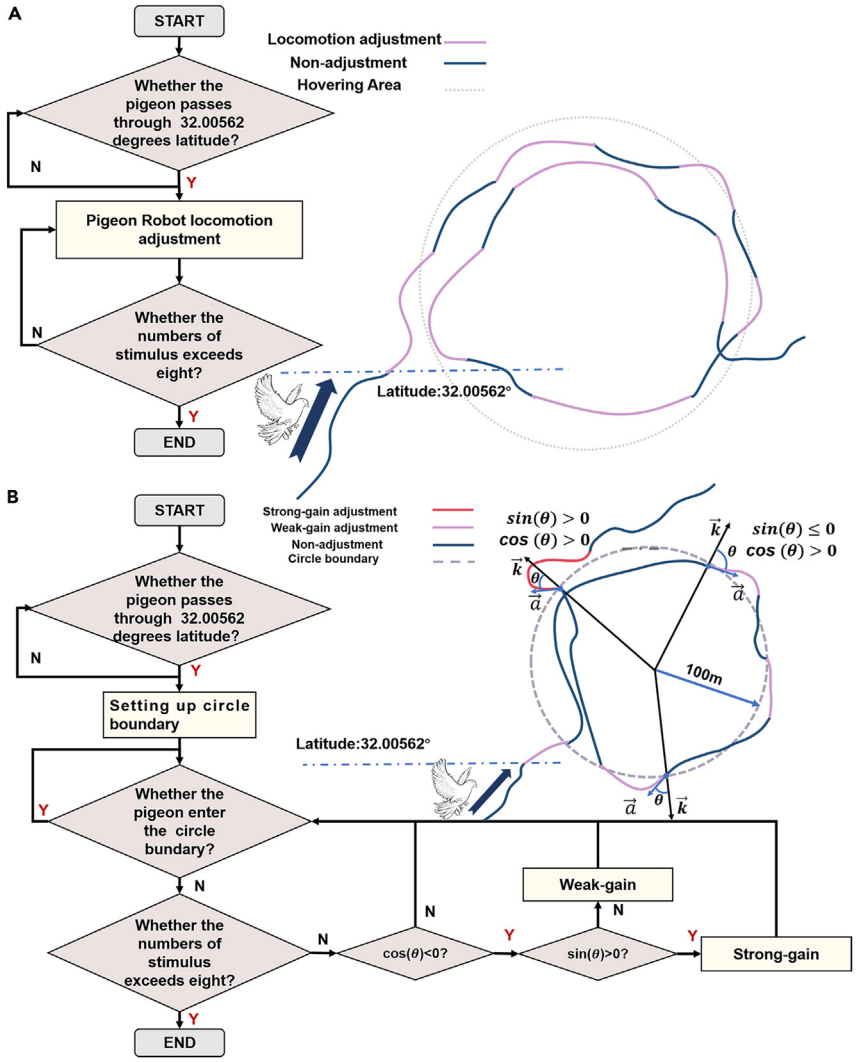

Figure 4. Schematic diagram of the hovering flights in outdoor experiments

(A) The fixed simulation paradigm and potential flight responses of subjects.

(B) The flexible stimulation paradigm. Here, θ indicates the angle between the normal vector (long black arrow, $\vec{k}$) and the head orientation (short blue arrow, $\vec{a}$) of the subject: (1) $\cos(\theta) < 0$, indicating flight trajectory toward the circle; (2) $\cos(\theta) > 0$ and $\sin(\theta) > 0$, indicating flight trajectory strongly deviates from the circle; (3) $\cos(\theta) > 0$ and $\sin(\theta) \leq 0$, indicating flight trajectory weak deviates from the circle.

For pigeon robots undergoing optogenetics navigation, for example, it needs 2 or 3 weeks to transduce the virus with its functional activity only maintaining for 3 months,[43,46] based on some of our previous work. Moreover, the temporal accuracy of chemogenetic stimulation for behavior regulations is relatively low, often taking hours, whereas the time resolution required for navigating hovering behavior in the field is often within seconds[36,42]. Additionally, optogenetics requires the use of high-power LEDs with fixed wavelength filters, which can be costly. During our field navigation experiments, the SGD acted as a consumable material, often becoming lost along with the pigeon. This could involve either losing the entire device but having the pigeon return, losing parts of the component, or the device being entirely broken. Therefore, considering the field navigation circumstance electrical stimulation is superior to others. In order to mitigate the widespread effects of electric stimulation and promote more precise results, in this work, we used an instruction set to customize the condition of individual pigeons and adapted by increasing the stimulation pulse width rather than elevating the stimulation amplitude to enhance navigation performance. Despite being considered an outdated method, electrical stimulation remains the most suitable and economical way to navigate pigeons in the field.

Moreover, the nucleus and network of brains are likely evolutionarily homologous between birds and mammals.[47] Anatomical structures of the central neural system can be roughly mapped to corresponding behaviors by using lesions, electrical stimulation, and genetic engineering. Accurately adjusted behaviors can be achieved largely by using different parameters of neuronal signals delivered to the related nuclei and networks. However, it is difficult for free-flying subjects to find causal relationships between behavioral patterns

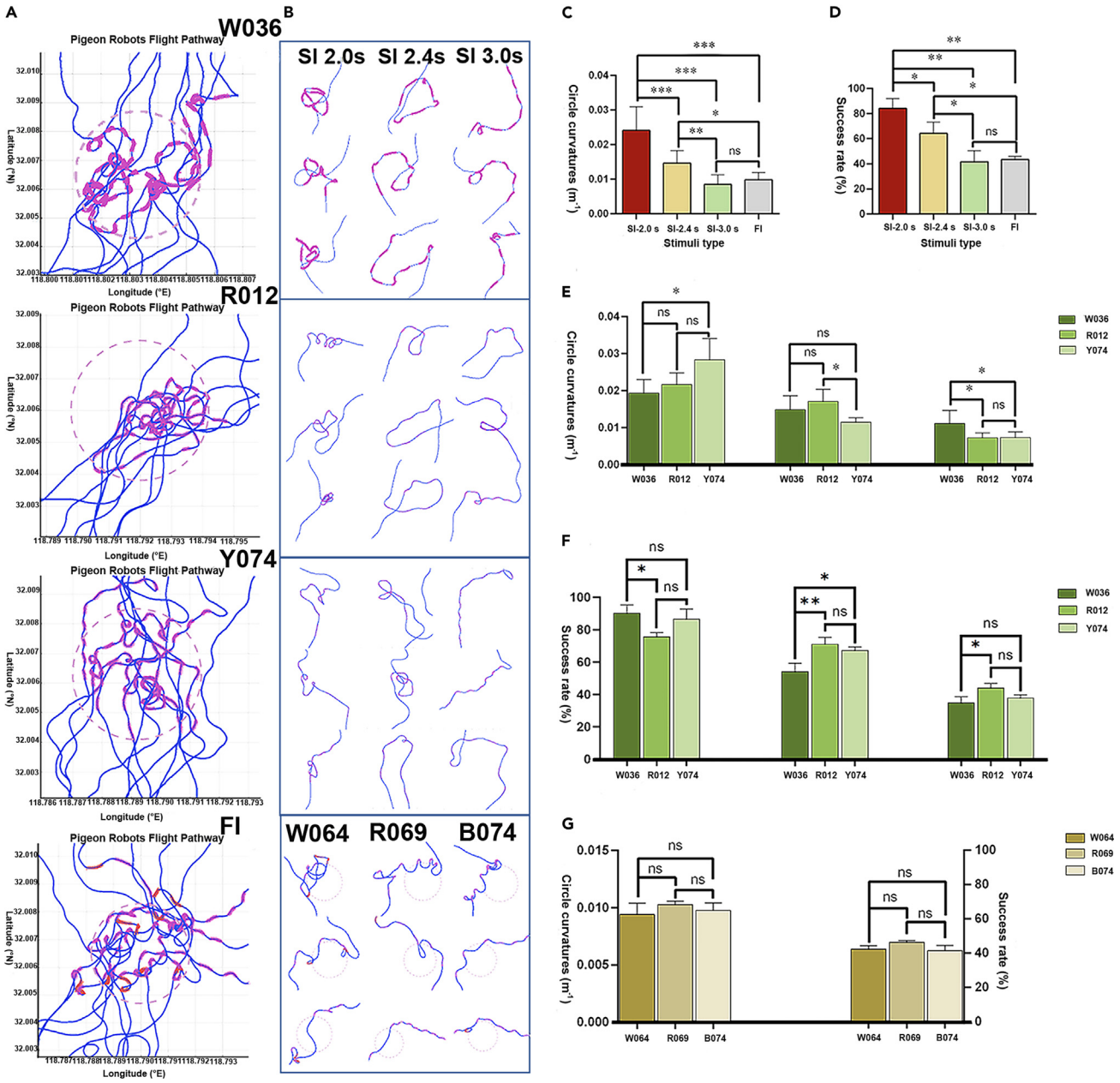

Figure 5. The hovering performance of pigeon robots driven by two stimulation procedures

(A) Overlapped drawings of individual hovering tracks.

(B) The same data presented individually.

(C and D) Pair comparisons of the circle curvatures and success rates in response to stimulus intervals of fixed 2 s, 2.4 s, 3 s, and flexible interval (FI), respectively.

(E and F) Individual variations in the circle curvatures and success rates in response to three fixed stimulus intervals.

(G) Less individual variations in the circle curvatures (left) and the success rates (right) under flexible stimulus intervals.

and/or degrees and the specific neuronal signals, because the quantitative measure of behavioral response to precise stimulus was conducted mostly in sedative animals under electromagnetic shielding. Alternatively, the artificial stimulation with different parameters or parameter sets of adjustable voltage, pulse width, duty cycle, and frequency were applied in discovering relationships between neural signals and corresponding pigeon flights in this work, providing a feasible approach to illuminate the identity of neural signals and specific motion behavior.[14] By using these adjustable artificial parameters, correlations between specific coefficients in the instruction set and specific behaviors could be established, indirectly decoding the transmission of motion information from upper to lower motor neurons.

Table 4. Effects of stimulus intervals (SIs) on circle curvature and success rate for procedure 1

Procedure 1	Stimulus interval	Sample	Average	*P*
Circle curvature (m^{-1})	2.0s	16	0.025	<0.001
	2.4s	16	0.015	
	3.0s	20	0.009	
–	Total	52	0.016	–
Success rate (%)	2.0s	16	87.5	0.021 < 0.05
	2.4s	16	75.0	
	3.0s	20	43.8	
–	Total	52	68.8	–

Upgraded devices for pigeon hovering control

Unlike other animal robots, SGD carried by the pigeon robot has been designed to collect three-dimensional posture and location information and adjust various moving behaviors.[34,37] The previous version of SGD we made could only measure the coordinates of latitude and longitude, which could not satisfy the demand for free flying in three dimensions. Therefore, SGD was upgraded by adding one barometer module to acquire height signals for calculating the altitude coordinate.[48] In addition, we optimized energy consumption to allow a long-term operation with the existing small battery volume in a compact size, involved in the energy-efficient core and peripheral components. Under the 400 mAh power condition, the older version of the SGD only worked for 3 h, while the upgraded version extended the duration to 6 h. In this work, we adapted the digital-to-analog converter (DAC) in the SGD to generate voltage from 0.01 V to 3.30 V. The older version of the SGD used only the pulse-width modulation (PWM) function to generate electric stimuli. With the upgraded SGD, we can adjust the stimulation voltage to accommodate individual pigeons by simply compiling the program, rather than changing the components in the circuit.

Moreover, previous SGDs mainly have two modes of information process: wireless remote transmission and per-programmed SD card.[14] With wireless transmission technology, the postures and locations of the pigeon were processed online in real-time. Nevertheless, the device demands a series of communication base stations along the pathway because the transportation range of radio signals is relatively limited at a restricted location. In addition, the fast-moving of the pigeon robots can result in data sampling loss.[15] Alternatively, the pre-programmed mode solves the aforementioned problems.[15] This paradigm's disadvantage is the inability to intervene online during the flight guidance process. Given the above issues, this study designed a micro-SGD with a pre-programmed module to collect, record and process the posture and location information of the pigeon robots in outdoor flight in real-time. With this upgraded SGD, pigeon robots were forced to hover within a given circle at the preset site could be efficiently completed under the control of procedure 2 which needs processed information on the posture and location on time.

Compared with previous devices,[17] our SGD has advantages in five features. (1) Switching stimulation could evoked automatically by the angle degree of the head orientation (STAR Methods) of the pigeon with the normal vector of the circle during the hovering. (2) Three-dimensional space was used to guide the flight. (3) Energy-efficient components extended significantly the operation duration. (4) An adjustable instruction set could customize individual pigeon robots. (5) Outdoor flights of pigeon robots could be adjusted to perform turning circles at the preset site.

Limitations of the study

All robots displayed behavioral similarities to each other while variations in response to different stimulation paradigms existed among individuals and trials, which provided a chance to analyze the relationship between the curvatures of the pigeon robot flight and turning success

Table 5. Individual difference in circle curvatures and success rates for procedure 2

Procedure 2	Pigeon robot	Sample	Average	*P*
Circle curvature (m^{-1})	W064	9	0.007	0.882 > 0.05
	R069	9	0.009	
	B074	8	0.008	
	total	26	0.008	–
Success rate (%)	W064	9	60.0	0.921 > 0.05
	R069	9	66.7	
	B074	8	50.0	
	total	26	59.8	–

rates.[10,19] The smaller the curvature hovered, the lower the success rate achieved. It is most likely that completing a small rotation would require a strong effort to overcome the inertia force created by turning. The same situation could be often observed in animals running on the ground.

The SI of 3s in procedure 1 could result in the same behavioral performances as procedure 2 did, much stable between individual pigeons than those with SIs of 2 s and 2.4 s. The animal vectors could benefit from the flexible stimulation pattern since the total stimulus dose was probably less than procedure 1. The less dose of stimulation the nerve system received, the weaker the brain trauma the animal sacrificed. Furthermore, procedure 1 could lead subjects to reduce the turning radius, gradually producing small-scale hovering. And procedure 2 prompts subjects to hover at a predetermined location. However, after having experienced a long SI in procedure 2, the possibility of accomplishing a full turning circle generally decreased. That meant the pigeon robots adjusted their flight postures spontaneously and flew toward the loft during the elongated SI period.

Unlike the laboratory stage, the flight behaviors of the pigeon robots in urban were more complex and difficult. For instance, the residential pattern, high-rised construction, and the avian flock in the flying route might contribute to the trajectory deviation of the pigeon robot. Therefore, it was difficult in outdoor controlled navigation to create the relationship between parameters and corresponding behaviors. For purposes of data reliability, repeatability, and fidelity, we focused on adjusting pigeon robots' fixed-point turning in the clockwise direction. Furthermore, to generalize our procedures, we successfully conducted three counterclockwise turnings for evidence that the pigeon robots were able to turn both directions (see Figure S6). Therefore, the methods employed in this research not only fix the pathway for the pigeon to avoid external influences but also use fixed and flexible procedures to mitigate individual differences in results. These methods served as a reference for other researchers seeking to navigate animals in the field.

Conclusion

The conclusions of this work involved six phases: (1) Selection of pigeon brain nuclei and histological verification; (2) construction and fabrication of an energy-efficiency device with space-time coordinates; (3) validation of locomotion control of pigeon robots in laboratory conditions; (4) creation of outdoor flight routes for each pigeon robot; (5) control of fixed-point hovering at preset sites under two procedures; (6) Establishment of relationships between stimulation parameters and circle curvature/hovering success rate. Based on the above mentioned, this research highlights several key points. First, the upgraded energy-efficient SGD extends operational hours, providing more opportunities to gather data in each trial. This work facilitated us to comprehensively understand the entire scene of stimuli guidance and hovering trajectory. Furthermore, the stimulus module of pulse width gain demonstrates effectiveness in both laboratory and field for turning navigation. Two procedures revealed the pros and cons of balancing individual differences and achieved a higher success rate. The results of this study could be valuable for future research on controlling the outdoor navigation of animal robots and could open new avenues for the development of animal robots.

RESOURCE AVAILABILITY

Lead contact

Further information or requests for reagents resources, and data should be addressed to the lead contact, Wenbo Wang (wwb523@nuaa.edu.cn).

Materials availability

This work did not generate new unique reagents and components.

This work did not generate new pigeon strains.

Data and code availability

- All raw data reported in this paper will be shared by the lead contact upon request.
- All custom-made scripts and codes for analysis are available for request by contacting the lead author, Wenbo Wang (wwb523@nuaa.edu.cn).
- Any additional information required to reanalyses the data reported or the detail for SGD designed in this paper is available from the lead contact upon request.

ACKNOWLEDGMENTS

This work was supported by the National Key Research and Development Program of China (grant no. 2020YFB1313504).

AUTHOR CONTRIBUTIONS

In the process of writing the article, all authors invested lots of time and energy. Among the authors in the list, W.W. and Z.D. designed research; Z.Z. performed research; Z.Z., R.L., and Y.T. analyzed and interpreted the data; Z.Z. and Y.T. wrote and edited the paper. And the corresponding author W.W. will hold responsibilities for lead contact.

DECLARATION OF INTERESTS

The authors declare no conflicts of interest.

STAR★METHODS

Detailed methods are provided in the online version of this paper and include the following:

- KEY RESOURCES TABLE
- EXPERIMENTAL MODEL AND SUBJECT DETAILS
  - Experimental animals
- METHOD DETAILS
  - Stereotaxic surgery for implantation and injection
  - Histology
  - Valid candidate for pigeon robots
  - Preparation process for flight
  - Pathway fixation
  - Navigation in open field
  - Navigation in field
- QUANTIFICATION AND STATISTICAL ANALYSIS
  - SGD function analysis
  - Pathway analysis
  - Head orientation analysis
  - Statistics analysis

SUPPLEMENTAL INFORMATION

Supplemental information can be found online at https://doi.org/10.1016/j.isci.2024.110927.

Received: January 18, 2024
Revised: June 11, 2024
Accepted: September 9, 2024
Published: September 11, 2024

REFERENCES

1. Zhou, Z., Liu, D., Sun, H., Xu, W., Tian, X., Li, X., Cheng, H., and Wang, Z. (2021). Pigeon Robot for Navigation Guided by Remote Control: System Construction and Functional Verification. J. Bionic Eng. *18*, 184–196. https://doi.org/10.1007/s42235-021-0013-3.
2. Wang, S., Shen, L., Liu, X., and Liao, H. (2016). A wearable backpack chip for honeybee biorobot. In 2016 China Semiconductor Technology International Conference (CSTIC) (IEEE), pp. 1–3. https://doi.org/10.1109/CSTIC.2016.7463917.
3. Nguyen, H.D., Tan, P., Sato, H., and Doan, T.T.V. (2019). Ultra-Lightweight Cyborg Insect: Sideways walking of remote-controlled living beetle with a miniature backpack. In 2019 IEEE International Conference on Cyborg and Bionic Systems (CBS) (IEEE), pp. 11–16. https://doi.org/10.1109/CBS46900.2019.9114394.
4. Zhang, S., Yuan, S., Huang, L., Zheng, X., Wu, Z., Xu, K., and Pan, G. (2019). Human Mind Control of Rat Cyborg's Continuous Locomotion with Wireless Brain-to-Brain Interface. Sci. Rep. *9*, 1321. https://doi.org/10.1038/s41598-018-36885-0.
5. Burton, A., Won, S.M., Sohrabi, A.K., Stuart, T., Amirhossein, A., Kim, J.U., Park, Y., Gabros, A., Rogers, J.A., Vitale, F., et al. (2021). Wireless, battery-free, and fully implantable electrical neurostimulation in freely moving rodents. Microsyst. Nanoeng. *7*, 62. https://doi.org/10.1038/s41378-021-00294-7.
6. Bozkurt, A., F Gilmour, R., Jr., and Lal, A. (2009). Balloon-Assisted Flight of Radio-Controlled Insect Biobots. IEEE Trans. Biomed. Eng. *56*, 2304–2307. https://doi.org/10.1109/TBME.2009.2022551.
7. Kobayashi, N., Yoshida, M., Matsumoto, N., and Uematsu, K. (2009). Artificial control of swimming in goldfish by brain stimulation: Confirmation of the midbrain nuclei as the swimming center. Neurosci. Lett. *452*, 42–46. https://doi.org/10.1016/j.neulet.2009.01.035.
8. Wenbo, W., Ce, G., Jiurong, S., and Zhendong, D. (2009). Locomotion Elicited by Electrical Stimulation in the Midbrain of the Lizard Gekko gecko. In Intelligent Unmanned Systems: Theory and Applications Studies in Computational Intelligence, A. Budiyono, B. Riyanto, and E. Joelianto, eds. (Springer Berlin Heidelberg), pp. 145–153. https://doi.org/10.1007/978-3-642-00264-9_9.
9. Yu, Y., Pan, G., Gong, Y., Xu, K., Zheng, N., Hua, W., Zheng, X., and Wu, Z. (2016). Intelligence-Augmented Rat Cyborgs in Maze Solving. PLoS One *11*, e0147754. https://doi.org/10.1371/journal.pone.0147754.
10. Khajei, S., Shalchyan, V., and Daliri, M.R. (2019). Ratbot navigation using deep brain stimulation in ventral posteromedial nucleus. Bioengineered *10*, 250–260. https://doi.org/10.1080/21655979.2019.1631103.
11. Sato, H., Peeri, Y., Baghoomian, E., Berry, C.W., and Maharbiz, M.M. (2009). Radio-Controlled Cyborg Beetles: A Radio-Frequency System for Insect Neural Flight Control. In 2009 IEEE 22nd International Conference on Micro Electro Mechanical Systems (IEEE), pp. 216–219. https://doi.org/10.1109/MEMSYS.2009.4805357.
12. Wang, Y., Lu, M., Wu, Z., Tian, L., Xu, K., Zheng, X., and Pan, G. (2015). Visual Cue-Guided Rat Cyborg for Automatic Navigation [Research Frontier]. IEEE Comput. Intell. Mag. *10*, 42–52. https://doi.org/10.1109/MCI.2015.2405318.
13. Xu, K., Zhang, J., Zhou, H., Lee, J.C.T., and Zheng, X. (2016). A novel turning behavior control method for rat-robot through the stimulation of ventral posteromedial thalamic nucleus. Behav. Brain Res. *298*, 150–157. https://doi.org/10.1016/j.bbr.2015.11.002.
14. Shim, S., Yun, S., Kim, S., Choi, G.J., Baek, C., Jang, J., Jung, Y., Sung, J., Park, J.H., Seo, K., et al. (2020). A handheld neural stimulation controller for avian navigation guided by remote control. BME *30*, 497–507. https://doi.org/10.3233/BME-191070.
15. Vyssotski, A.L., Serkov, A.N., Itskov, P.M., Dell'Omo, G., Latanov, A.V., Wolfer, D.P., and Lipp, H.-P. (2006). Miniature Neurologgers for Flying Pigeons: Multichannel EEG and Action and Field Potentials in Combination With GPS Recording. J. Neurophysiol. *95*, 1263–1273. https://doi.org/10.1152/jn.00879.2005.
16. Cao, F., Zhang, C., Choo, H.Y., and Sato, H. (2016). Insect–computer hybrid legged robot with user-adjustable speed, step length and walking gait. J. R. Soc. Interface *13*, 20160060. https://doi.org/10.1098/rsif.2016.0060.
17. Cai, L., Dai, Z., Wang, W., Wang, H., and Tang, Y. (2015). Modulating Motor Behaviors by Electrical Stimulation of Specific Nuclei in Pigeons. J. Bionic Eng. *12*, 555–564. https://doi.org/10.1016/S1672-6529(14)60145-1.
18. Mouritsen, H., Heyers, D., and Güntürkün, O. (2016). The Neural Basis of Long-Distance Navigation in Birds. Annu. Rev. Physiol. *78*, 133–154. https://doi.org/10.1146/annurev-physiol-021115-105054.
19. Xu, W., Yang, L., Wang, Z., Yang, L., Cheng, H., Zhu, S., Shang, Z., and Wang, Z. (2023). Stratum Griseum Periventriculare-mediated Fear Emotion Regulates Motor Behavior in Pigeons. J. Bionic Eng. *20*, 2228–2239. https://doi.org/10.1007/s42235-023-00382-6.
20. Tian, X., Gong, Z., Zhang, Y., Xu, W., Liu, H., Zhou, Z., Liu, D., and Wang, Z. (2020). The impact of tag position and mass on motor behavior in pigeons. J. Ornithol. *161*, 1167–1174. https://doi.org/10.1007/s10336-020-01798-1.
21. Garcia-Rill, E., Skinner, R.D., Jackson, M.B., and Smith, M.M. (1983). Connections of the mesencephalic locomotor region (MLR) I.

Substantia nigra afferents. Brain Res. Bull. *10*, 57–62. https://doi.org/10.1016/0361-9230(83)90075-8.

22. Garcia-Rill, E., Skinner, R.D., Gilmore, S.A., and Owings, R. (1983). Connections of the mesencephalic locomotor region (MLR) II. Afferents and efferents. Brain Res. Bull. *10*, 63–71. https://doi.org/10.1016/0361-9230(83)90076-X.
23. Dautan, D., Kovács, A., Bayasgalan, T., Diaz-Acevedo, M.A., Pal, B., and Mena-Segovia, J. (2021). Modulation of motor behavior by the mesencephalic locomotor region. Cell Rep. *36*, 109594. https://doi.org/10.1016/j.celrep.2021.109594.
24. Jones, B.E., and Yang, T.Z. (1985). The efferent projections from the reticular formation and the locus coeruleus studied by anterograde and retrograde axonal transport in the rat. J. Comp. Neurol. *242*, 56–92. https://doi.org/10.1002/cne.902420105.
25. Noga, B.R., and Whelan, P.J. (2022). The Mesencephalic Locomotor Region: Beyond Locomotor Control. Front. Neural Circ. *16*, 884785. https://doi.org/10.3389/fncir.2022.884785.
26. Schwarz, L.A., and Luo, L. (2015). Organization of the Locus Coeruleus-Norepinephrine System. Curr. Biol. *25*, R1051–R1056. https://doi.org/10.1016/j.cub.2015.09.039.
27. Manger, P.R., and Eschenko, O. (2021). The Mammalian Locus Coeruleus Complex—Consistencies and Variances in Nuclear Organization. Brain Sci. *11*, 1486. https://doi.org/10.3390/brainsci11111486.
28. Guglielmone, R., and Panzica, G.C. (1982). Topographic, morphologic and developmental characterization of the nucleus loci coerulei in the chicken: A Golgi and fluorescence-histochemical study. Cell Tissue Res. *225*, 95–110. https://doi.org/10.1007/BF00216221.
29. Carter, M.E., Yizhar, O., Chikahisa, S., Nguyen, H., Adamantidis, A., Nishino, S., Deisseroth, K., and De Lecea, L. (2010). Tuning arousal with optogenetic modulation of locus coeruleus neurons. Nat. Neurosci. *13*, 1526–1533. https://doi.org/10.1038/nn.2682.
30. Ferreira-Pinto, M.J., Kanodia, H., Falasconi, A., Sigrist, M., Esposito, M.S., and Arber, S. (2021). Functional diversity for body actions in the mesencephalic locomotor region. Cell *184*, 4564–4578.e18. https://doi.org/10.1016/j.cell.2021.07.002.
31. Inagaki, H.K., Chen, S., Ridder, M.C., Sah, P., Li, N., Yang, Z., Hasanbegovic, H., Gao, Z., Gerfen, C.R., and Svoboda, K. (2022). A midbrain-thalamus-cortex circuit reorganizes cortical dynamics to initiate movement. Cell *185*, 1065–1081.e23. https://doi.org/10.1016/j.cell.2022.02.006.
32. Wang, S., Wang, Z., and Mu, Y. (2022). Locus Coeruleus in Non-Mammalian Vertebrates. Brain Sci. *12*, 134. https://doi.org/10.3390/brainsci12020134.
33. Benarroch, E.E. (2018). Locus coeruleus. Cell Tissue Res. *373*, 221–232. https://doi.org/10.1007/s00441-017-2649-1.
34. Xu, S., Talwar, S.K., Hawley, E.S., Li, L., and Chapin, J.K. (2004). A multi-channel telemetry system for brain microstimulation in freely roaming animals. J. Neurosci. Methods *133*, 57–63. https://doi.org/10.1016/j.jneumeth.2003.09.012.
35. Guo, S.C., Zhou, H., Wang, Y.M., Zheng, X.X., and Xu, K.D. (2013). A Rat-Robot Control System Based on Optogenetics. AMM *461*, 848–852. https://doi.org/10.4028/www.scientific.net/AMM.461.848.
36. Zhou, Z., Mei, H., Li, R., Wang, C., Fang, K., Wang, W., Tang, Y., and Dai, Z. (2022). Progresses of animal robots: A historical review and perspectiveness. Heliyon *8*, e11499. https://doi.org/10.1016/j.heliyon.2022.e11499.
37. Sato, H., Berry, C.W., Casey, B.E., Lavella, G., Ying, Y., VandenBrooks, J.M., and Maharbiz, M.M. (2008). A cyborg beetle: Insect flight control through an implantable, tetherless microsystem. In 2008 IEEE 21st International Conference on Micro Electro Mechanical Systems (IEEE), pp. 164–167. https://doi.org/10.1109/MEMSYS.2008.4443618.
38. Herculano-Houzel, S. (2020). Birds do have a brain cortex—and think. Science *369*, 1567–1568. https://doi.org/10.1126/science.abe0536.
39. von Eugen, K., Endepols, H., Drzezga, A., Neumaier, B., Güntürkün, O., Backes, H., and Ströckens, F. (2022). Avian neurons consume three times less glucose than mammalian neurons. Curr. Biol. *32*, 4306–4313.e4. https://doi.org/10.1016/j.cub.2022.07.070.
40. Josset, N., Roussel, M., Lemieux, M., Lafrance-Zoubga, D., Rastqar, A., and Bretzner, F. (2018). Distinct Contributions of Mesencephalic Locomotor Region Nuclei to Locomotor Control in the Freely Behaving Mouse. Curr. Biol. *28*, 884–901.e3. https://doi.org/10.1016/j.cub.2018.02.007.
41. Powell, S.K., Samulski, R.J., and McCown, T.J. (2020). AAV Capsid-Promoter Interactions Determine CNS Cell-Selective Gene Expression In Vivo. Mol. Ther. *28*, 1373–1380. https://doi.org/10.1016/j.ymthe.2020.03.007.
42. Liu, Q., Wu, Y., Wang, H., Jia, F., and Xu, F. (2022). Viral Tools for Neural Circuit Tracing. Neurosci. Bull. *38*, 1508–1518. https://doi.org/10.1007/s12264-022-00949-z.
43. Düring, D.N., Dittrich, F., Rocha, M.D., Tachibana, R.O., Mori, C., Okanoya, K., Boehringer, R., Ehret, B., Grewe, B.F., Gerber, S., et al. (2020). Fast Retrograde Access to Projection Neuron Circuits Underlying Vocal Learning in Songbirds. Cell Rep. *33*, 108364. https://doi.org/10.1016/j.celrep.2020.108364.
44. Rook, N., Tuff, J.M., Isparta, S., Masseck, O.A., Herlitze, S., Güntürkün, O., and Pusch, R. (2021). AAV1 is the optimal viral vector for optogenetic experiments in pigeons (Columba livia). Commun. Biol. *4*, 100. https://doi.org/10.1038/s42003-020-01595-9.
45. Sánchez-Valpuesta, M., Suzuki, Y., Shibata, Y., Toji, N., Ji, Y., Afrin, N., Asogwa, C.N., Kojima, I., Mizuguchi, D., Kojima, S., et al. (2019). Corticobasal ganglia projecting neurons are required for juvenile vocal learning but not for adult vocal plasticity in songbirds. Proc. Natl. Acad. Sci. USA *116*, 22833–22843. https://doi.org/10.1073/pnas.1913575116.
46. Hisey, E., Kearney, M.G., and Mooney, R. (2018). A common neural circuit mechanism for internally guided and externally reinforced forms of motor learning. Nat. Neurosci. *21*, 589–597. https://doi.org/10.1038/s41593-018-0092-6.
47. Medina, L. (2007). Do Birds and Reptiles Possess Homologues of Mammalian Visual, Somatosensory, and Motor Cortices? In Evolution of Nervous Systems (Elsevier), pp. 163–194. https://doi.org/10.1016/B0-12-370878-8/00132-4.
48. Yang, J., Huai, R., Wang, H., Li, W., Wang, Z., Sui, M., and Su, X. (2017). Global Positioning System-Based Stimulation for Robo-Pigeons in Open Space. Front. Neurorob. *11*, 40. https://doi.org/10.3389/fnbot.2017.00040.
49. Wei, K., and Kording, K.P. (2018). Behavioral tracking gets real. Nat. Neurosci. *21*, 1146–1147. https://doi.org/10.1038/s41593-018-0215-0.
50. Choo, H.Y., Li, Y., Cao, F., and Sato, H. (2016). Electrical Stimulation of Coleopteran Muscle for Initiating Flight. PLoS One *11*, e0151808. https://doi.org/10.1371/journal.pone.0151808.
51. Cole, J., Mohammadzadeh, F., Bollinger, C., Latif, T., Bozkurt, A., and Lobaton, E. (2017). A study on motion mode identification for cyborg roaches. In 2017 IEEE International Conference on Acoustics, Speech and Signal Processing (ICASSP) (IEEE), pp. 2652–2656. https://doi.org/10.1109/ICASSP.2017.7952637.

STAR★METHODS

KEY RESOURCES TABLE

REAGENT or RESOURCE RESOURCE	SOURCE	IDENTIFIER
REAGENT		
Phosphate Buffer Solution	Biosharp	(biosharp.cn)
Paraformaldehyde	XiGene	_Xigene (xigenebio.com)
SAKURA	Tissue-Tek O.C.T. Compound	Tissue-Tek O.C.T. Compound | O.C.T. Compound | Sakura Finetek USA (sakuraus.com)
Fluoro-Gold	Fluorochrome	FluoroGold™ | CAS 223769-64-0 | SCBT - Santa Cruz Biotechnology
Other (Electron Component)		
0.1uF	C1,C3,C6,C7,C9,C10,C17, C20,C21,C22,C23,C24	N/A
10uF	C2,C16,C18	N/A
22pF	C4,C5	N/A
4.7uF	C8	N/A
1uF	C11,C13,C14,C15	N/A
4.7pF	C12	N/A
TF-021B-H265	CARD1	SOFNG
1N5819	D1,D2,D3,D8	DIODES
HDR-F-1.27_1X5	H1	N/A
SH1.0-6P	J1	N/A
82nH	L1	Sunlord
10uH	L3	N/A
PH2.0-2P	P3	N/A
LED	PWR1,STU1,STU2	EVERLIGHT
1M	R1,R10,R12	N/A
1K	R2,R3,R7,R8	N/A
45K	R4,R5,R6,R9	N/A
130K	R11	N/A
10K	R13	N/A
4.7K	R14,R17,R20	N/A
0Ω	R18,R19	FH
STM32L151CCU6	U1	STMicroelectronics
LT1615ES5-1#TRPBF	U2	LINEAR
BST-BMP390L	U3	N/A
ADG5404BRUZ-REEL7	U4	Analog Devices
IPX	U7	N/A
LT6015IS5#TRPBF	U8	ADI/LINEAR
ME6217C33M5G	U9	Nanjing Micro One Elec
8M	Y1	N/A
ATK-BlU	Blue-tooth	ALIENTEK
TAU1202A	U5	N/A

(*Continued on next page*)

Continued

REAGENT or RESOURCE RESOURCE	SOURCE	IDENTIFIER
Deposited data		
Raw and analyzed data	This paper	https://data.mendeley.com/preview/pckndfgm36?a=16c10a53-3d7d-43f9-b53e-795281485415
Experimental models: Organisms/strains		
Pigeon	Local market	N/A
Software and algorithms		
MATLAB	Math Works	Version 2021a
OlyVIA	Olympus	N/A
Photoshop	Adobe	Version 5
Altium Designer	PCB-Design	Altium Designer - PCB Design Software
keil uvision5	arm keil	Keil Embedded Development Tools for Arm, Cortex-M, Cortex-R4, 8051, C166, and 251 processor families.
GraphPad PRISM (v7.0)	GraphPad PRISM	Home - GraphPad
pycharm	JETBRAINS	PyCharm: The Python IDE for data science and web development by JetBrains
Deeplabcut	Mathis et al., (2018): https://doi.org/10.1038/s41593-018-0209-y,[49]	https://github.com/DeepLabCut/DeepLabCut

EXPERIMENTAL MODEL AND SUBJECT DETAILS

Experimental animals

This study selected adult male and female pigeons with weights 350g–450g as vectors for constructing the animal robots. All efforts were made to minimize animal suffering, such as that the surgical procedures were performed under general anesthesia (0.00135 mL/g). Our works were approved by the Jiangsu Association for Laboratory Animal Science (Jiangsu, China).

The pigeons were housed in a dovecote with a natural light-dark cycle, and their navigational behaviors were presented during the mildness and calm light phase. All pigeons received sufficient water and cereal to support their daily lives. Each pigeon was implanted with the electrodes, and housed in a single cage. Pigeons were allowed to conduct a maximum of once trail a day or participate in behavior verification for up to 30 min per day.

METHOD DETAILS

Stereotaxic surgery for implantation and injection

All surgical procedures were performed under aseptic conditions. Pigeons were anesthetized using pentobarbital sodium (0.00135 mL/g) and placed in a stereotaxic apparatus. Electrode implantation was performed in the midbrain, with two electrodes implanted in symmetrical FRM and the others in symmetrical LoC. During the surgical procedures, our aim was to implant four 130μm diameter electrodes into specific nuclei. First, the borehole and fixed two medical nickel-metal self-tapping screws was made to stabilize the electrodes interface. Then, an irregular pattern on the skull was made with a cranial drill to facilitate later fixation with dental cement. Thereafter, the holes in the skull were drilled according to the implantation site's, while the drilling diameter at approximately 0.3 mm to reduce additional injury. Finally, under the guidance of the three-dimensional stereotactic locator, we implanted the electrodes at a slow, constantly speed. After completing the operation, we sewed the wound area and applied triple antibiotic ointment evenly around the wound for healing. Besides, fluoresce-gold (FG) concentration at 4% was dissolved in 0.9% salt water and injected into the midbrain at the same sites as the electrode implantation to verify. After the general anesthesia took effect, holes same as electrode implantation were drilled on the skull. Then, the glass electrode (inner diameter 0.54 mm, outer diameter 1.14 mm, without inner core) was slowly and constantly implanted into FRM and LoC, and 1μL FG was injected. The Vet-bond Tissue Adhesive was adapted to occlude the hole in the skull. Then, the wound area was sewed and healing. After ten days for expression, the pigeons were sacrificed for certification.

Histology

The fluoresce-gold (FG) was adopted to verify the electrode canal location. Ten days after the FG injection, animals were first perfused with phosphate buffer saline (PBS) and then fixed using a 4% paraformaldehyde (PFA) solution. The brains were harvested and placed in PFA (4%) for 8 h, soaked in 30% sucrose solution for 48 h, then sectioning 50-μm slices in the coronal plane using a freezing microtome (Leica CM1950,

Germany). Sections were examined under a research-grade whole slide scanning system (Olympus VS200, Japan) to verify the fluorescent markers (DiI fluorescence) of electrode placement within the FRM and LoC (see Figure S2). The stability and reliability of this work on the behavior and posture regulation of the pigeon robot were confirmed histologically (see Table S1).

Valid candidate for pigeon robots

After the pigeon has recovered from the electrode implantation surgical operation, we employed two criteria to assess whether the individual pigeon could be utilized in subsequent analyses (see Figures S1B and S1C). 1) All implanted sites were capable of inducing the desired behavioral response under a threshold of electrical stimulation set at 1.0 V, along with a duty cycle of 50%, pulse width of 0.5 ms, and frequency of 80 Hz. 2) The pigeon was able to perform a round with a fixed point in the open field using the instructed pulse width (0.5 ms), frequency (80 Hz), and ensuring that the stimulation amplitude did not exceed 3.0 V. The purpose of these two criteria is 2-fold: to select individual pigeons capable of effectiveness under the instruction sets' guidance and to test the optimized stimulation amplitude for sequential guidance.

Preparation process for flight

Our dovecote was located at the Ming Palace Campus of Nanjing University of Aeronautics and Astronautics. The pigeons were taken out from the dovecote at the Ming Palace Campus and transported by shuttle bus to the Jiangjun Road Campus, where they were released, every calm and mild morning (between 7:10 a.m. and 8:00 a.m.). Before releasing, the GPS coordinates and relative altitude coordinates were calibrated using the SGD and placed in a backpack on the pigeon's dorsal. Then, in the afternoon (at 5:00 p.m.), the SGDs were retrieved from the pigeon's backpack in the dovecote.

Pathway fixation

The new trainee pigeons were paired with experienced homing pigeons to learn and fix the homing pathway. Each new recruit was paired with an experienced pigeon and released together. If the new pigeon did not return with the experienced pigeon, it would be eliminated (considered lost or returned on its own in the following days, within the first 3 trials). Each trainee pigeon underwent 20 training flights, with 14 flights accompanied by experienced pigeons. Additionally, the trajectories of the 6 flights that the trainee pigeons completed on their own were recorded and analyzed.

Navigation in open field

All indoor behavior-control experiments were conducted in an open field (1.26 m × 1.26 m × 0.45 m) fenced in the laboratory. The field was divided into four rectangular sections to label the pigeons' locations, with a square at a corner set as the fixed start site (see Figure S4A). A block was placed at the center of the field to prevent pigeons from taking shortcuts during navigation. To avoid external distractions for the pigeons in the laboratory, the open field was illuminated by natural white (4500K–5500K) LEDs and covered with one-way light transmission film (see Figure S4A).

For the verification of electrode implantation, pigeons were placed at the center of the open field in an awake, free-moving state after recovering from surgery. After a 15-min accommodation period, the pigeons underwent electrical stimulation with an instruction set of 1.0 V, 1 s duration, 0.5 ms pulse width, and 50% duty cycle to test their response.

For the optimization of stimulus parameters, pigeons were placed at the center of the open field, and the initial setup of the instruction set was the same as for the verification of the electrode implantation. (see Figures S5A–S5C) Then, the voltage was incrementally increased step by step until the pigeon could perform a circle turning $\geq 360^{\circ}$, following the approach outlined in previous research.[10,50,51] This voltage was considered as the optimized stimulus parameter. For the PW gain verification, pigeons were placed at the fixed start site in the open field with the center block, and the initial setup of the instruction set was the same as the individual's own optimized voltage parameter. Then, the PW was incrementally increased step by step to 0.5 ms, 0.7 ms, and 0.9 ms to compel the pigeon to move around the center block for one circle, recording the stimuli times (see Figures S4B–S4D).

Navigation in field

Procedure 1

Procedure 1 involved three pigeon robots, W036, R012, and Y074, with relative fixation routes after training. The trigger boundary for hovering control was set at latitude coordinate 32.00562° on their homing pathway. The pigeon robots were adjusted continuously for their flight trajectories when passing through the trigger boundary. In procedure 1, the pigeon robots that complete a 300° turning were considered successful hovering. The pigeon robots would be taken off duty right after total electrical stimuli reached eight times to avoid neuronal injury from excessive dose of electrical shocks. (Figure 4A). The stimulation parameters were set as follows: 80Hz bipolar square wave with the optimized voltage, which resulted from laboratory tests for each pigeon robot; the initial PW set at 0.5ms and increased with 0.1ms step after each stimulation to decrease neural habituation; stimulation duration 3s with SI 2–3 s; total stimuli fixed to eight times for spontaneous posture adjustment of the pigeon robots.

Procedure 2

To promote the pigeon robots performing delicate circle flights in a relatively restrictive location, flexible interval (FI) procedure 2 was designed based on the results from procedure 1 with the rest of the pigeon robots W064, R069, and B074. Two stimulation categories were intended; one was 0.5 ms duration with 0.1 ms increase step named as weak PW stimuli, and another was 0.5 ms duration with 0.2 ms increase step as substantial PW stimuli. To restrict the hovering flights within a designed radius, the circle boundary with 100m radius was applied in procedure 2. The trigger boundary was set at 120m away from the center of the circle, creating a 20m buffer distance for pigeon robots in response to stimulation (Figure 4B). If the robot flew toward the designed circle, no stimulation would be applied, while its trajectory was not toward the circle, a weak stimulus was provided to guide it into the circle. Once pigeon exceeded the circle boundary, a weak PW stimulus was provided if the angle of the head orientation of the pigeon with the normal vector of the circle was smaller than 90° while a substantial PW stimuli was applied if the angle bigger than 90°. The rest parameters of stimulation and determination of success were the same as those in procedure 1. Ultimately, the effects of SIs on the circle curvature and hovering success rate were compared statistically between the FI in procedure 2 and each SI in procedure 1. The schematic diagrams of the overall navigation strategy of the second procedure were presented in Figure 4B.

QUANTIFICATION AND STATISTICAL ANALYSIS

SGD function analysis

First we verified the stimulus signal generation part by using oscilloscope detect the resolution (Equation 1). The default output voltage range of the D/A conversion module is 0 to V_{REF+}. Based on the reference voltage input V_{REF+} = 3.3V of the current device, the output accuracy (resolution) of the D/A conversion module can be calculated as follows:

$$R_{es} = V_{REF+}/2^{12} = 3.3V/2^{12} = 0.000804V = 0.804mV \quad \text{(Equation 1)}$$

Given that the conversion time (Tc) of the analog signal is 4us (Equation 2), the conversion rate of the D/A conversion module can be calculated as follows:

$$V_{es} = 1/T_c = 1/4\mu s = 250KHZ \quad \text{(Equation 2)}$$

Next, the posture acquisition part was verified. While the GPS model is commercial off-the-shelf, the air pressure sensor required algorithmic correction. During pigeon movement, the sensitivity of the air pressure sensor dynamically changed due to acceleration. Changing altitude rapidly, the air pressure sensor fluctuates significantly. To maintain the stability of the pressure sensor, a first-order dynamic low-pass filtering algorithm was adapted to calibrate the current altitude data. This algorithm weighs the altitude data collected at the previous time A_o and the altitude data collected at the current time A_n (Equation 4).While the altitude variation is more than 50 m/s, the dynamic weighting coefficient is 0; whereas, when the altitude variation does not exceed 50 m/s, the dynamic weighting coefficient is K_x (Equation 3). And the relative altitude was calculated as follows:

$$K_x = exp\wedge|A_n - A_o| / 25 \quad \text{(Equation 3)}$$

$$A_n = A_o + K_x(A_{n-1} - A_{o-1}) \quad \text{(Equation 4)}$$

Pathway analysis

During the pathway analysis, the longitude and latitude coordinates were needed to convert into ground coordinates to obtain the actual distance. Then, the Euclidean distance of flight pathways was calculated, and the length of the path was obtained through, while S_{lo} represents the longitude coordinates (Equation 5) and S_{la} represents the latitude (Equation 6) coordinates, both recorded by the SGD. The ground coordinate unit (m) was obtained after the conversion of latitude and longitude coordinates, and the final flight pathway was obtained the sum of the Euclidean distance (Equation 7).

$$y_i = S_{lo_i} \times 111000 \quad \text{(Equation 5)}$$

$$x_i = S_{la_i} \times 111000 \times cos(S_{la_i}) \quad \text{(Equation 6)}$$

$$d = \sum_{i=1}^{n} \sqrt{(x_i - x_{i-1})^2 + (y_i - y_{i-1})^2} \quad \text{(Equation 7)}$$

Head orientation analysis

Judging whether the pigeon's hovering exceeds the circle boundary and applying the weak-gain or strong-gain at each stimuli, we introduce the variables $\vec{a}$, $\vec{k}$, and θ to calculate the hovering state based on the longitude and latitude coordinates. After the pigeon arrives at the trigger boundary, we first utilize the following formulas to analyze the latitude and longitude numerically.

While the pigeon robots exceed the circle boundary, by analyzing the relationship between the positive and negative value of $sin(\overrightarrow{k}, \overrightarrow{a})$ and $cos(\overrightarrow{k}, \overrightarrow{a})$ ($\overrightarrow{a}$ means the direction vector difference between the current position and the previous position of the pigeon robot; $\overrightarrow{k}$ means the normal vector of the circle boundary.), three flight states of the pigeon robot were defined. 1) While $cos(\overrightarrow{k}, \overrightarrow{a}) \leq 0$ it is considered that the pigeon robot is flying toward the circle boundary, and the behavior navigation of the pigeon robot is absent; 2) While $cos(\overrightarrow{k}, \overrightarrow{a}) > 0$ and $sin(\overrightarrow{k}, \overrightarrow{a}) > 0$ it is considered that the pigeon robot is flying away from the circle boundary, and the flight direction deviated from the clockwise tangent direction of the circle boundary by more than 90°. Under this condition, the P.W. gain from the stimulation signal needs to expand to add extra 0.2ms after each stimulation; 3) While $sin(\overrightarrow{k}, \overrightarrow{a}) \leq 0$ it is considered that the pigeon robot flying away from the circle boundary, and the flight direction deviated from the clockwise tangent direction of the circle boundary by less than 90°.

For clockwise navigation of the pigeon robot, the following formula was adapted. When the pigeon robots exceed the circle boundary, the relationship between the positive and negative values of $sin(\overrightarrow{k}, \overrightarrow{a})$ and $cos(\overrightarrow{k}, \overrightarrow{a})$ was analyzed to define three flight states of the pigeon robot: 2) While $cos(\overrightarrow{k}, \overrightarrow{a}) \geq 0$ it is considered that the pigeon robot is flying toward the circle boundary, and the behavior navigation of the pigeon robot is absent; 2) While $cos(\overrightarrow{k}, \overrightarrow{a}) < 0$ and $sin(\overrightarrow{k}, \overrightarrow{a}) > 0$ it is considered that the pigeon robot is flying away from the circle boundary, and the flight direction deviated from the clockwise tangent direction of the circle boundary by more than 90°. Under this condition, the P.W. gain from the stimulation signal needs to expand to add an extra 0.2ms after each stimulation; 3) while $sin(\overrightarrow{k}, \overrightarrow{a}) \leq 0$ it is considered that the pigeon robot is flying away from the circle boundary, and the flight direction deviated from the clockwise tangent direction of the circle boundary by less than 90°.

Success rate as (Equation 8):

$$Success\ rate = success/total \times 100\% \quad \text{(Equation 8)}$$

Circle curvature (Equation 9):

$$K = \Delta\theta \Big/ \Delta s = tan\left(\overrightarrow{k}, \overrightarrow{a}\right) \Big/ \sum_{i=1}^{n} \sqrt{(x_i - x_{i-1})^2 + (y_i - y_{i-1})^2} \quad \text{(Equation 9)}$$

Statistics analysis

The standard deviations of the flight trajectory lengths in the last 6 training trials were analyzed using standard deviation analysis, with all standard deviations found to be less than 1. The pulse widths (PWs) modulation and trajectory lengths deviations for individual pigeons were analyzed using one-way ANOVA. The success rates and circle curvature between and within the fixed stimulus procedure and flexible stimulus procedure were calculated using one-way ANOVA. Statistical significance was considered for $*p < 0.05$, $**p < 0.01$ and $***p < 0.001$. Detailed statistical information for all experiments is included in their corresponding figure legends.